S-NPP VIIRS Thermal Emissive Band Gain Correction during the Blackbody Warm-Up-Cool-Down Cycle

Taeyoung Choi*[a], Changyong Cao[b], and Fuzhong Weng[b]

[a] Earth Resource Technology, Inc.
[b]NOAA Center for Satellite Applications and Research,

ABSTRACT

The Suomi National Polar orbiting Partnership (S-NPP) Visible Infrared Imaging Radiometer Suite (VIIRS) has on-board calibrators called blackbody (BB) and Space View (SV) for Thermal Emissive Band (TEB) radiometric calibration. In normal operation, the BB temperature is set to 292.5 K providing one radiance level. From the NOAA's Integrated Calibration and Validation System (ICVS) monitoring system, the TEB calibration factors (F-factors) have been trended and show very stable responses, however the BB Warm-Up-Cool-Down (WUCD) cycles provide detectors' gain and temperature dependent sensitivity measurements. Since the launch of S-NPP, the NOAA Sea Surface Temperature (SST) group noticed unexpected global SST anomalies during the WUCD cycles. In this study, the TEB F-factors are calculated during the WUCD cycle on June 17th 2015. The TEB F-factors are analyzed by identifying the VIIRS On-Board Calibrator Intermediate Product (OBCIP) files to be Warm-Up or Cool-Down granules. To correct the SST anomaly, an F-factor correction parameter is calculated by the modified C1 (or b1) values which are derived from the linear portion of C1 coefficient during the WUCD. The F-factor correction factors are applied back to the original VIIRS SST bands showing significantly reducing the F-factor changes. Obvious improvements are observed in M12, M14 and M16, but corrections effects are hardly seen in M16. Further investigation is needed to find out the source of the F-factor oscillations during the WUCD.

Keywords: S-NPP, VIIRS, Thermal Band, Blackbody, F-factor, Warm Up Cool Down, Sea Surface Temperature

1. INTRODUCTION

As a major instrument onboard the Suomi National Polar-orbiting Partnership (S-NPP) satellite, the Visible Infrared Imaging Radiometer Suite (VIIRS) was launched on October 28, 2011 opening the nadir door on November 21, 2011. The S-NPP satellite is in a Sun-synchronous near-circular polar orbit with an approximate equator passing time of 1:30 P.M. in an ascending node at an altitude of 829 km [1]. It orbits the Earth about 14 or 15 times per day providing radiometric products in radiance and/or reflectance scales depending on the band of interest. To provide scientific grade of data quality, VIIRS uses improved sensor and on-board calibrations with calibration back traceable to the prelaunch references followed by the Moderate resolution Imaging Spectroradiometer (MODIS) design [2]. Similar but improved sensor design with the lessons learned from MODIS experience, VIIRS has a Rotating Telescope Assembly (RTA) and the Half Angle Mirror (HAM) derotator in the path of the incoming radiation path. Similar to MODIS, it also includes a series of On-Board Calibrators (OBC) that are blackbody (BB), solar diffuser (SD), solar diffuser stability monitor (SDSM), and space view (SV). The calibration source of the mid-wave and long-wave infrared bands is BB and SV within a wavelength range from 3.7 to 12 μm, whereas the SD, SDM, and SV are used for reflective solar bands (RSB) within a wavelength range between 0.4 to 2.25 μm. After the S-NPP launch, the early lifetime on-orbit performance assessment results validated the health of the instrument and VIIRS met the specification with excellent signal to noise ratio [1]. On March 2014, the VIIRS Sensor Data Record (SDR) products achieved the validated maturity status, which means the VIIRS SDR were well measured and its quality satisfied the expected quality within the specifications [3] [4]. Even after reaching to the validated maturity, there were residual striping patterns along with the scan direction in the sea surface temperature (SST) environmental data record (EDR) products [5]. The source of striping was well characterized by using SD and it was caused by nosier detector 1 and 2 in M15 and detector 9 in M16 [6]. In addition to

*taeyoung.choi@noaa.gov; phone 1-301-683-3562; STAR / NESDIS / NOAA

Earth Observing Systems XXI, edited by James J. Butler, Xiaoxiong (Jack) Xiong, Xingfa Gu, Proc. of SPIE
Vol. 9972, 99721J · © 2016 SPIE · CCC code: 0277-786X/16/$18 · doi: 10.1117/12.2236995

the scan direction striping issues, SST group reported approximately 0.3K spikes in the SST anomalies during the quarterly WUCD cycles as shown in Figure 1 [7].

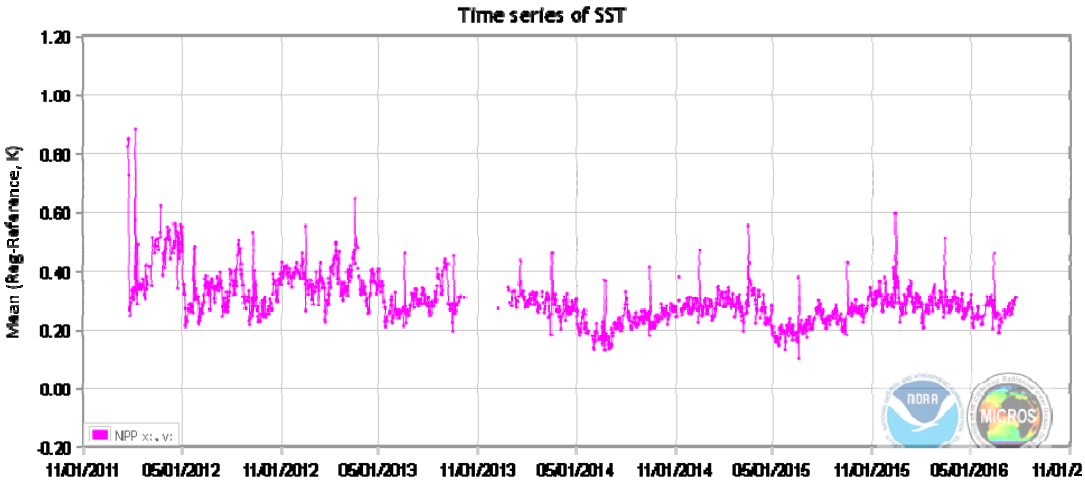

Figure 1. S-NPP VIIRS time series SST from NOAA Monitoring of IR Clear-sly Radiances over Oceans for SST (MICROS) site at http://www.star.nesdis.noaa.gov/sod/sst/micros/.

For TEB calibration, the BB is in a normal operational temperature at 292.5K which provides one radiance level of calibration point. The BB WUCD cycles has been performed every three months starting from warming up sequence with the pre-determined plateaus up to 315.9K. After reaching the top plateau, the BB goes into cooling down sequence with a minimum plateau at 272.5K. During the WUCD cycles, the TEB calibration coefficients (F-factors) were supposed to be stable in theory, however, the F-factor fluctuations has been observed in the near real-time monitoring system called Integrated Calibration and Validation System (ICVS) (at http://www.star.nesdis.noaa.gov/icvs/status_NPP_VIIRS.php).

Instead of using F-factors, the linear portion of C1 coefficient (which is identical to b1 coefficient in the MODIS TEB calibration) is re-calculate during a WUCD cycle on Jun 17, 2015. To differentiate the C coefficient, the recalculated C1 coefficient is named as b1 coefficient and calculated by using the pre-launch C0 and C2 coefficients from the C look-up-table (LUT). The new b1 coefficient was re-applied back to the original F-factor equation based on the ratio correction from the normal BB temperature to correct the F-factor variations during the WUCD cycles.

2. ON-ORBIT TEB CALIBRATION

Details of on-orbit TEB calibration equation development and descriptions are well documented in the Joint Polar Satellite System (JPSS) VIIRS radiometric calibration algorithm theoretical basis document (ATBD) [8]. Following explanations summarized the TEB calibration steps along with the essential equations.

The TEB equation starts with the background bias removed digital number (dn) between the BB and SV (dn_{BB}) or Earth View (EV) and SV (dn_{SV}) as shown in Equation 1 below.

$$dn_{BB} = DN_{BB} - DN_{SV} \quad (1)$$

The capital DN denotes the digital number before the bias (or background) removal and the lower case dn indicates a bias corrected digital number. The major source of the TEB calibration is BB and its signal observed by VIIRS is denoted as L_{BB} and it is shown in Equation 2.

$$L_{BB\_AP} = \varepsilon L_{BB} + (1-\varepsilon)(F_{RTA}L_{RTA} + F_{SH}L_{SH} + F_{CAV}L_{CAV}) \quad (2)$$

The L_{BB_AP} is the BB radiance at the BB aperture and it is based on the Planck spectral radiance at the BB temperature with emissivity of ε. The $(1-\varepsilon)$ term denotes reflectivity of the BB and they are combined with three difference weighting terms from RTA, BB shield, and cavity that are denoted as F_{RTA}, F_{SH}, and F_{CAV}, respectively. All these components are calculated by their own temperatures with the Planck spectral radiance. The spectral radiance at a measured temperature is averaged over the relative spectral radiance in each spectral band in Equation 3.

$$L_i = \frac{\int_{\lambda\_start}^{\lambda\_end} L_i(\lambda) RSR(\lambda) d\lambda}{\int_{\lambda\_start}^{\lambda\_end} RSR(\lambda) d\lambda} \quad (3)$$

Another component of the *dn* signal is the self-emission residual background term, L_{BG}, which is calculated by following Equation (4).

$$L_{BKG} = \frac{\left[(1-\rho_{RTA})L_{RTA} - L_{HAM}\right]}{\rho_{RTA}} \quad (4)$$

In Equation 4, the ρ_{RTA} is the RTA reflectivity and L_{RTA} and L_{HAM} are Planck function applied spectral radiance with the RTA and HAM temperatures. Finally, the TEB calibration coefficient, F-factor, is calculated as shown in Equation 5.

$$F = \frac{(RVS_{BB} - RVS_{SV})L_{BKG} + RVS_{BB} \cdot L_{BB\_AP}}{c_0 + c_1 \cdot dn_{BB} + c_1 \cdot dn_{BB}^2} \quad (5)$$

The pre-determined response versus scan angle (RVS) is characterized by the prelaunch calibration at the SV, SD, BB, and all the EV angles. Since the BB observation is made at the BB observation angle, the RVSBB is applied in Equation 5. The differences between the RVS_{BB} and RVS_{SV} are corrected in the equation, where the background emission differences are corrected by the BB and SV observation angles. Once we have the F-factor, at aperture spectral radiance, L_{EV_AP} , from the EV port can be calculated by Equation 6 applying C coefficient and F-factor along with the residual background term.

$$L_{EV\_AP} = \frac{F \cdot (c_0 + c_1 \cdot dn_{BB} + c_1 \cdot dn_{BB}^2) - (RVS_{EV} - RVS_{SV})L_{BKG}}{RVS_{EV}} \quad (6)$$

3. RESULTS

Long-term On-orbit TEB F-factor Trending

The on-orbit long-term F-factor trending results are calculated based on the Onboard Calibrator Intermediate Product (OBCIP) files produced by the Interface Data Processing Segment (IDPS). One OBCIP file is chosen per orbit when the S-NPP spacecraft is transition from the night to day mode. The TEB F-factors are calculated using the same OBCIP granules that are used for RSB calibration for consistency and comparability. The Figure 2 shows band averaged TEB F-factor in the ICVS webpage at http://www.star.nesdis.noaa.gov/icvs/status_NPP_VIIRS.php.

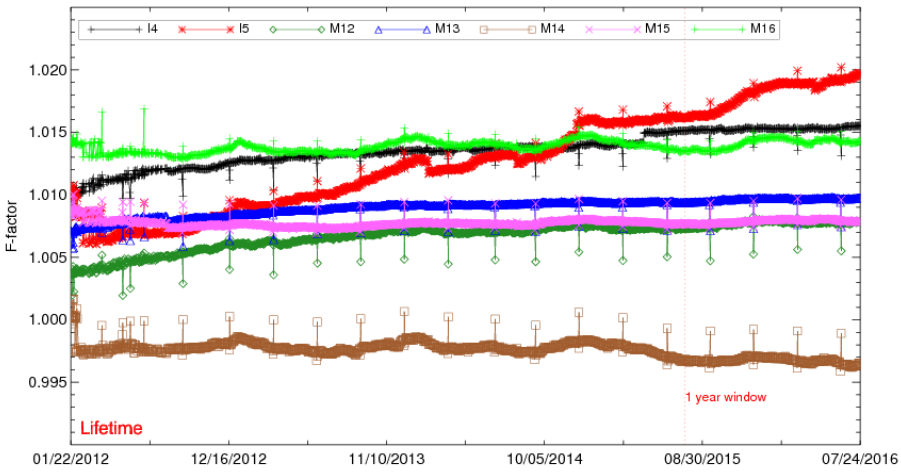

Figure 2. S-NPP VIIRS Band averaged TEB F-factors.

In the band averaged TEB F-factor plot, each symbol represents a daily averaged F-factor and there are some discontinuous points especially in I5. These discontinuous points are caused by sudden changes in the bias removed dn. Besides discontinuity in I5, the most noticeable thing in all the bands is the periodic vertical lines in the F-factors. These vertical lines have been caused by the quarterly WUCD events. Other than the WUCD related spikes, the F-factors are fairly stable over the lifetime especially in the SST related bands of M14, M15, and M16.

TEB F-factor During WUCD

In this study, we focused on a TEB WUCD event on 6/17/2015 especially within the SST related bands of M14, M15 and M16. Figure 3 shows the BB temperature from 6/17~6/19/2015 with the 5 temperature plateaus during the warm-up cycle at 297.5, 302.5, 307.5, 312.5, and 315.0K. And then the BB heater is turned off for 24 hours cooling down. When the BB temperature reaches to a stable minimum temperature level, BB heater is turned on and set to 272.5, 282.5, and finally set to 292.5K. The last temperature setting 292.5K is the default BB nominal temperature.

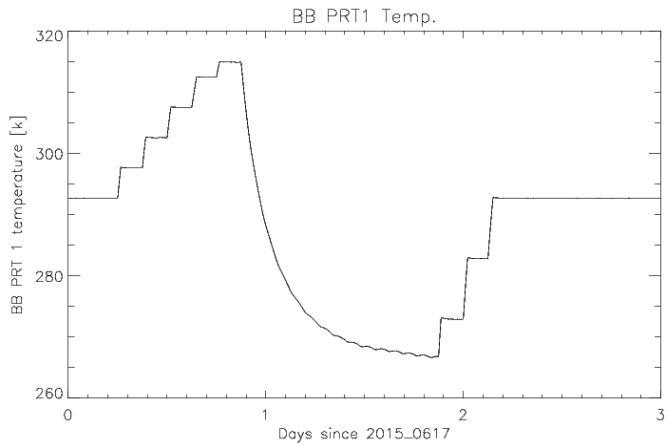

Figure 3. S-NPP VIIRS BB temperature profile from PRT1 during three days of WUCD cycle starting from 6/17/2015.

During a WUCD cycle, many parameters were tested and characterized such as noise equivalent delta temperature (NEdT) especially at the typical temperature, C coefficient derivation, and F-factor stability test. An early lifetime study

showed that the NEdT met the specifications with wide margin and the C coefficients were agreeing well with prelaunch results within 0.8% on average [2]. In their work, there were some room for improvements in TEB calibration algorithm since they observed an orbital cycle of F-factor variations on the order of 0.1 percent of discrepancy between offset driven on-orbit and prelaunch results. This F-factor problem is still in the TEB calibration as shown as F-factor variations during a WUCD cycle in Figure 4.

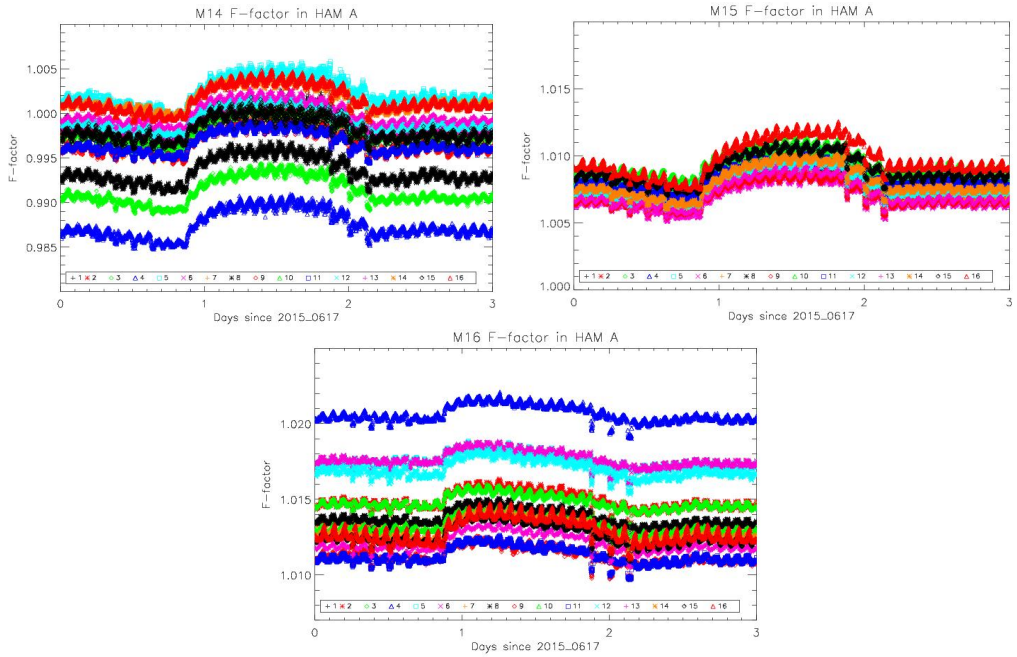

Figure 4. S-NPP VIIRS detector dependent F-factors in HAM A during three days of WUCD cycle starting from 6/17/2015.

TEB b1 coefficient calculation during WUCD

The C1 coefficient is a linear term which is the major contributor of the VIIRS observed radiance in the F-factor equation (Equation 5). Similar to the MODIS calibration, the on-orbit b1 coefficients are derived from the F-factor equation by setting the F=1 and C0 and C2 coefficients are calculated from the pre-launch LUT as shown in Equation (7) below. The on-orbit b1 coefficient trending plots in the SST bands are also shown in Figure 5.

$$b_1 = \left[\begin{array}{l} (RVS_{BB} - RVS_{SV}) \cdot \left[\dfrac{(1-\rho_{RTA})L_{RTA} - L_{HAM}}{\rho_{RTA}} \right] + \\ RVS_{BB} \left\{ \varepsilon L_{BB} + (1-\varepsilon)(F_{RTA}L_{RTA} + F_{BB\_SH}L_{BB\_SH} + F_{CAV}L_{CAV}) \right\} - c_0 - c_2 \cdot dn_{BB}^2 \end{array} \right] / (dn) \qquad (7)$$

The b1 coefficient trending plots in Figure 5 only shows averaged over the detectors with in HAM side A only. The shapes of b1 coefficient changes in the SST bands are strongly correlated to the BB temperature in Figure 3. The b1 transition pattern during the WUCD cycle shows negative correlation with the BB temperature in bands M14 and M15, whereas M16 shows positive correlation only during the warm-up (WU) cycle. Figure 6 shows relationship between the on-orbit b1 coefficient and BB temperature. The red symbols represent the b1 coefficients during the WU cycle, whereas the blue symbols represent the b1 during the CD cycle. The black vertical line which is a cluster of many symbols represents the BB plateaus during the WUCD cycles. As we expected, M14 and M15 show strong negative relationship between the b1 and BB temperature with negative slopes, however, there are different behavior between the WU and CD cycles. The different behaviors of the on-orbit b1 coefficients are modeled by independent quadratic function fits as shown in Figure 6. The response in band M16 does not show any significant correlation during the CD cycle but it has a

sign of positive correlation during the WU cycle. These strong relationships between the on-orbit b1 coefficient and BB temperature are used for an empirical correction factor development.

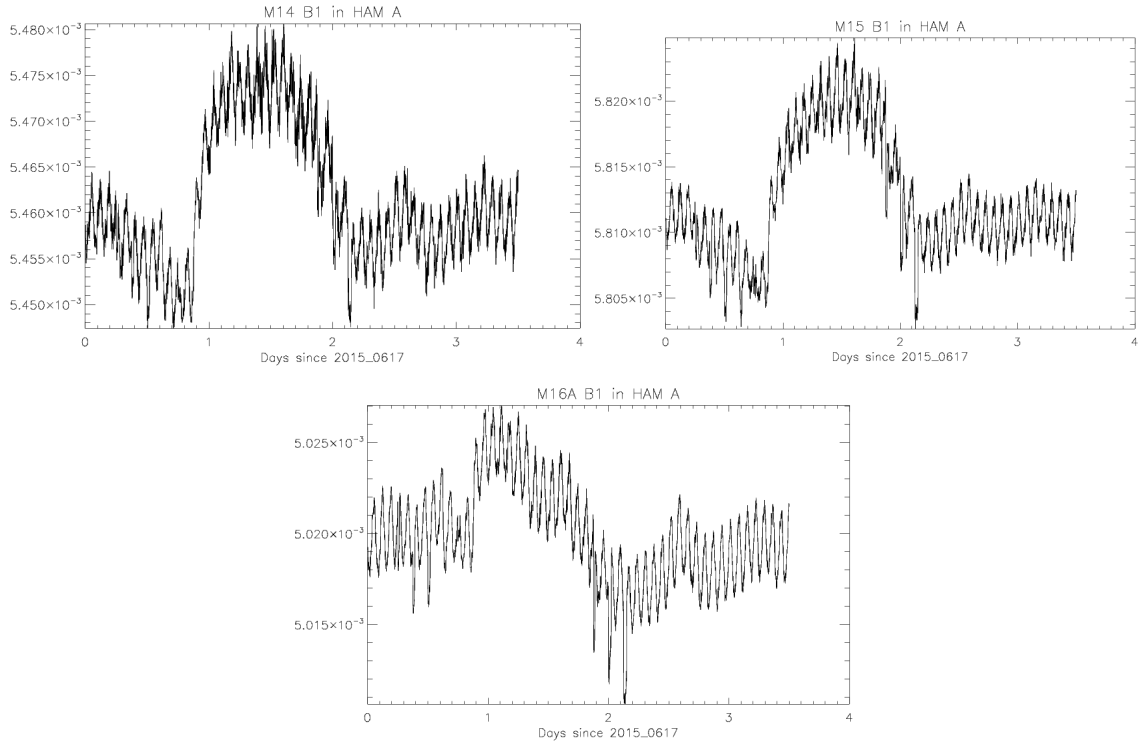

Figure 5. S-NPP VIIRS on-orbit b1 trending within HAM side A only during three days of WUCD cycle starting from 6/17/2015.

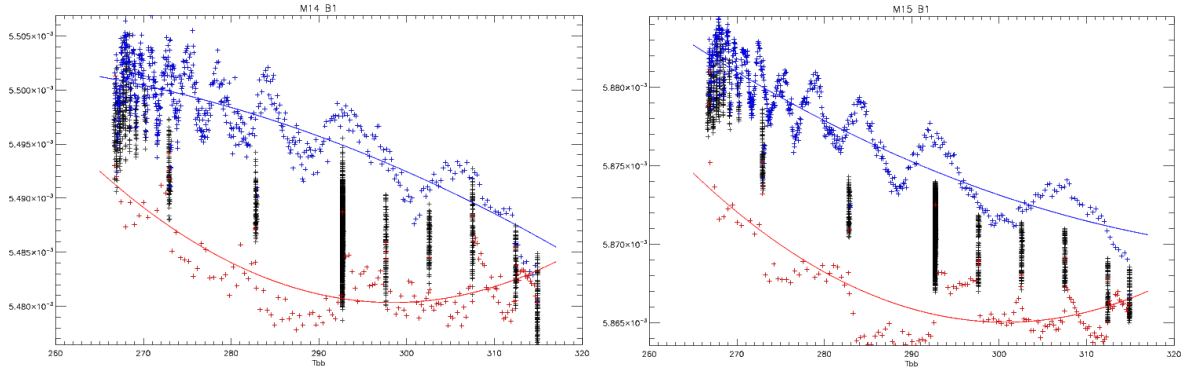

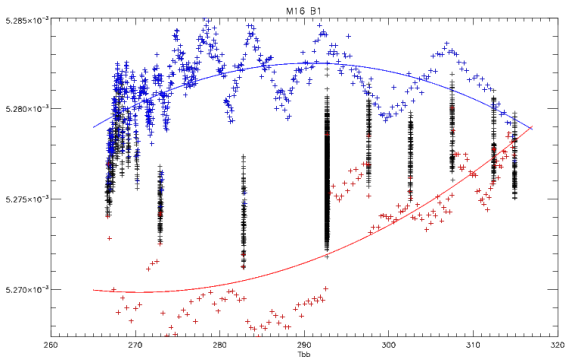

Figure 6. S-NPP VIIRS on-orbit b1 trending within HAM side A only during three days of WUCD cycle starting from 6/17/2015.

TEB correction back to F-factor during WUCD

Equation 8 shows an adjusted C1 coefficient during only within the WUCD cycle using the correlation relationships found between the on-orbit b1 coefficient and BB temperature. The quadratic correction factor, $fit(T_{BB})$, is developed independently within WU or CD cycle and applied back to the original F-factor equation. This ratio correction method is only applied to the SST bands and the results are shown in Figure 7. For clear comparisons, the before and after F-factor correction plots are placed side-by-side.

$$F = \frac{(RVS_{BB} - RVS_{SV}) \cdot \left[\frac{(1-\rho_{RTA})L_{RTA} - L_{HAM}}{\rho_{RTA}} \right] + RVS_{BB} \left\{ \varepsilon L_{BB} + (1-\varepsilon)(F_{RTA}L_{RTA} + F_{BB\_SH}L_{BB\_SH} + F_{CAV}L_{CAV}) \right\}}{c_0 + c_1 \cdot fit(T_{BB}) / fit(292.67K) \cdot dn_{BB} + c_2 \cdot dn_{BB}^2} \quad (8)$$

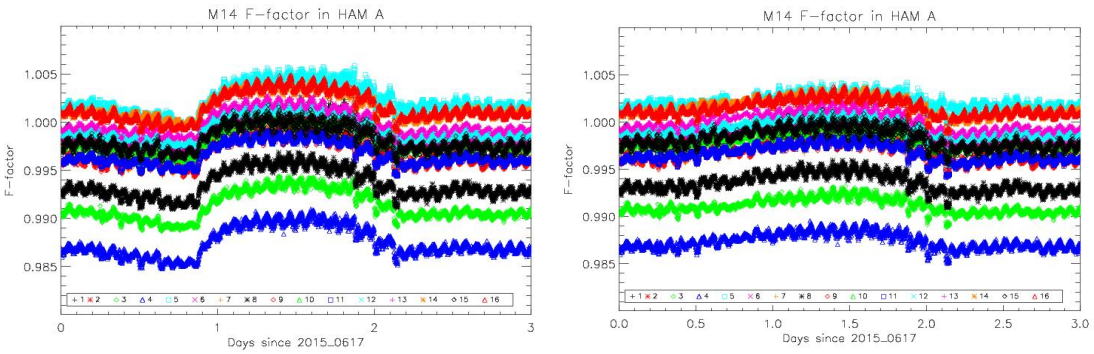

(a) M14 original F-factor (b) M14 after the b1 correction

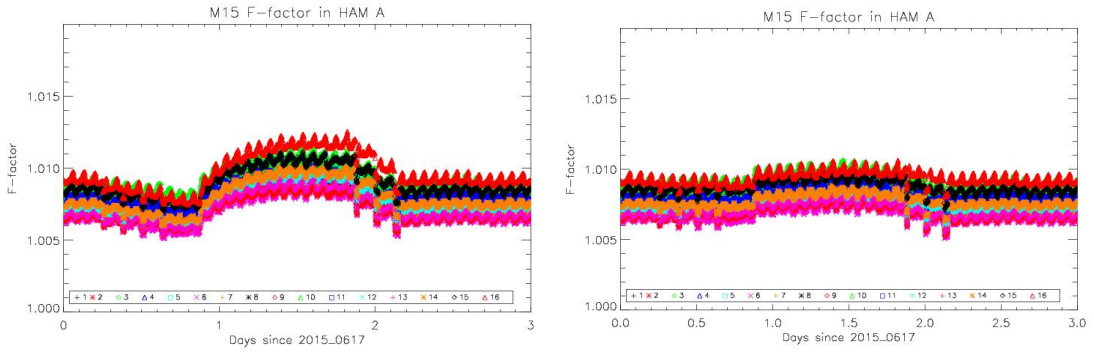

(a) M15 original F-factor (b) M15 after the b1 correction

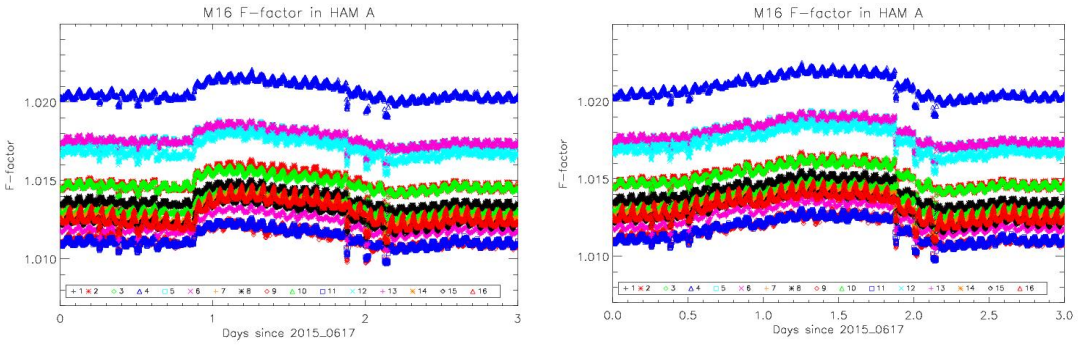

(a) M16 original F-factor

(b) M16 after the b1 correction

Figure 7. S-NPP VIIRS on-orbit b1 correction on F-facto in HAM side A only.

As shown in Figure 7, the F-factor correction did not completely removed the WUCD effects but the level of correction in M14 and M15 is significant that we can recognize the differences. During the WUCD cycle, the percent levels of the original F-factor changes were approximately 0.45, 0.40, and 0.2 percent in bands M14, M15, and M16, respectively. The b1 ratio correction during the WUCD reduced the levels of F-factor changes to 0.25 and 0.10 percent in M14 and M15; however, the M16 didn't show any improvement. The poor performance of the M16 correction was already expected in Figure 6 with the weak correlation between the on-orbit b1 coefficient and BB temperature.

4. SUMMARY

The on-orbit TEB radiometric coefficient, F-factor, has been successfully implemented and monitored by the NOAA's ICVS system. In all the TEB bands, the F-factors are very stable over the lifetime of S-NPP VIIRS but the quarterly BB WUCD caused unexpected global SST anomalies. Using a specific WUCD event on June 17, 2015, the F-Factors were calculated and they showed BB temperature related variations. To correct this WUCD related F-factor changes, on-orbit b1 coefficients were calculated by setting F=1 and using prelaunch C0 and C2 values from the LUTs. Within the SST bands (M14, M15, and M16), a set of b1 correction factors were developed and applied back to the original F-factors. The b1 correction factors were independently developed and applied during WU and CD cycles. The b1 based F-factor correction partially improved the F-factor changes in the SST bands. After the correction, the F-factors variations were reduced from 0.45 to 0.25 percent in band M14 and from 0.40 to 0.10 percent in band M15. NOAA VIIRS team is continuously monitoring the TEB F-factor and actively investigating the source of F-factor variations during the WUCD cycles to improve the quality of the NOAA's SDR products.

REFERENCES

[1] C. Cao, J. Xiong, S. Blonski, Q. Liu, S. Uprety, X. Shao, Y. Bai, and F. Weng, "Suomi NPP VIIRS sensor data record verification, validation, and long-term performance monitoring," *J. Geophys. Res. Atmos.*, vol. 118, no. 20, pp. 11664–11678, 2013.

[2] B. Efremova, J. Mcintire, D. Moyer, A. Wu, X. Xiong, B. Efremova, J. Mcintire, D. Moyer, A. Wu, and X. Xiong, "S-NPP VIIRS thermal emissive bands on-orbit calibration and performance," *J. Geophys. Res. Atmos. J. Geophys. Res. Atmos*, vol. 119, 2014.

[3] C. Cao, F. J. De Luccia, X. Xiong, R. Wolfe, and F. Weng, "Early on-orbit performance of the visible infrared imaging radiometer suite onboard the suomi national polar-orbiting partnership (S-NPP) satellite," *IEEE Trans. Geosci. Remote Sens.*, vol. 52, no. 2, pp. 1142–1156, 2014.

[4] C. Moeller, D. Tobin, G. Quinn, U. Wisconsin, and W. D. Street, "S-NPP VIIRS thermal band spectral radiance performance through 18 months of operation on-orbit," *Proc. SPIE 8866, Earth Obs. Syst. XVIII*, vol. 88661N, 2013.

[5] M. Bouali and A. Ignatov, "Adaptive reduction of striping for improved sea surface temperature imagery from Suomi National Polar-Orbiting Partnership (S-NPP) Visible Infrared Imaging Radiometer Suite (VIIRS)," *J. Atmos. Ocean. Technol.*, vol. 31, no. 1, pp. 150–163, 2014.

[6] T. Choi, C. Cao, and F. Weng, "Analysis of VIIRS TEB Noise Using Solar Diffuser Measurements," *Proc. SPIE 9607, Earth Obs. Syst. XX*, vol. 9607, pp. 1–12, 2015.

[7] A. Ignatov, Y. K. John Stroup, Xinjia Zhou, Boris Petrenko, Y. D. Prasanjit Dash, Xingming Liang, Kai He, and J. D. Liam Gumley, Steve Dutcher, "S-NPP VIIRS SST Reanalysis Version 1," in *NOAA S-NPP Reprocessing Worshop*, 2016.

[8] N. Baker, "Joint Polar Satellite System (JPSS) VIIRS Earth Gridding Algorithm Theoretical Basis Document (ATBD) For Public Release," p. 94, 2014.